Design and Evaluation of a Cable-Actuated Palletizing Robot With Geared Rolling Joints

Wontae Choi, *Student Member, IEEE*, and Jungwook Suh, *Member, IEEE*

***Abstract*—In the structure of a palletizing robot, auxiliary links are generally used to drive rotational links and maintain the horizontal orientation of the robot end-effector. However, with recent developments in manufacturing technologies and the increasing diversity of tasks, there is a demand for reducing the space occupied by auxiliary links with lightweight robot designs. In this article, a new method to reduce the size and weight of palletizing robots by replacing the existing auxiliary links with cable-actuation is proposed. First, the kinematics of a palletizing robot with parallelogram linkages based on geared rolling joints is explained. Additionally, the effects of multiple cable windings on the joint speed reduction are examined. A theoretical analysis of the relationship between the joint angle and cable length confirms that serially connected geared parallelograms can decouple joint motion. Furthermore, the effect of the cable length from the motor to the actuation joint on the stiffness is analyzed. Finally, experiments are conducted using a manufactured robot prototype to verify the effectiveness of cable windings, decoupled joint motion, and robot stiffness, and to confirm the accuracy of distal position and orientation. Consequently, the proposed cable-actuated palletizing robot is expected to be applied in various industrial robot designs.**

***Index Terms*—Actuation and joint mechanism, mechanism design, palletizing robot, rolling joint, tendon/wire mechanism.**

I. Introduction

IN VARIOUS industrial fields, robots have replaced human labor in repetitive tasks to improve production efficiency. These robots generally consist of vertical articulated structures and follow a serial configuration, where actuators are directly connected to each joint of the robot. However, in simple palletizing tasks that do not require multi-degree-of-freedom (DOF) movement of the end-effector, the heavy actuators located at the joints can decrease the robot's operational efficiency [1]. To improve this, palletizing robots have been developed with actuators placed near the base part. This structure reduces the weight and inertia of the robot arms, thereby ensuring energy efficiency and high payload capacities [2], [3].

Palletizing robots generally feature a 4-DOF parallel structure, which enables energy efficiency, high positional accuracy, and repeatability. These features are crucial in precision manufacturing and automation industries. In logistics and production lines, palletizing robots are commonly used to perform repetitive tasks, such as stacking, unstacking, and pick-and-place operations [4]. In terms of structural configuration, these robots utilize two or more auxiliary links to drive rotational links while maintaining the horizontal orientation of the distal links [5]. This design simplifies control, increases the robot arm stiffness, and extends the reachable range of distal links. However, the auxiliary links do not provide a separate speed reduction effect, and a thick link structure is required to achieve high payload capacity. Therefore, the auxiliary links occupy unnecessary space within the robot, which limits the reachable workspace and increases the risk of collision. Considering this aspect, several studies have attempted to replace the auxiliary links with timing belts to actuate the distal joints [6], [7]. However, limitations persist, particularly during high-load tasks, even when the stiffness has been increased by using metal pins and synthetic fibers inside the belt.

To address this problem, a cable-actuation mechanism can effectively replace the auxiliary links or timing belts in existing palletizing robots. Steel cables offer several advantages, such as low cost and flexible motion, and can enable the design of a lightweight robot [8], [9], [10]. Additionally, using a parallel structure with cables can facilitate the placement of heavy actuators at the base, thereby reducing the robot's inertia [11], [12], [13]. Moreover, unlike auxiliary links and timing belts, which lack significant speed reduction effects, cables can be wound around the multiple idle pulleys to amplify motor torque and robot stiffness [14], [15]. However, applying cables into existing pivot joints presents structural limitations, which complicates achieving the desired speed reduction effect [16].

In this article, a new method for improving the structure of a palletizing robot is proposed. A cable-actuated geared rolling joint is specifically applied to amplify the motor torque and stiffness, as well as to achieve decoupled motion of the joint, and enable a lightweight design. To verify the effectiveness of this structure, serially connected rolling-based parallelogram linkages are utilized. In these parallelograms, cable-actuated rolling joints enable independent joint motion. This feature

Manuscript received 20 January 2024; revised 6 April 2024; accepted 10 May 2024. Date of publication 6 June 2024; date of current version 16 August 2024. Recommended by Technical Editor Q. Zou and Senior Editor Q. Zou. This work was supported in part by the National Research Foundation of Korea Grant and in part by the Institute of Information and Communications Technology Planning and Evaluation grants funded by the Korea government under Grant NRF-2020-R1C1C1008707, Grant 2022-0-00501, and Grant RS-2023-00224546. *(Corresponding author: Jungwook Suh.)*

The authors are with the Department of Robot and Smart System Engineering, Kyungpook National University (KNU), Daegu 41566, South Korea (e-mail: wtchoi@knu.ac.kr; jwsuh@knu.ac.kr).

Color versions of one or more figures in this article are available at https://doi.org/10.1109/TMECH.2024.3403131.

Digital Object Identifier 10.1109/TMECH.2024.3403131

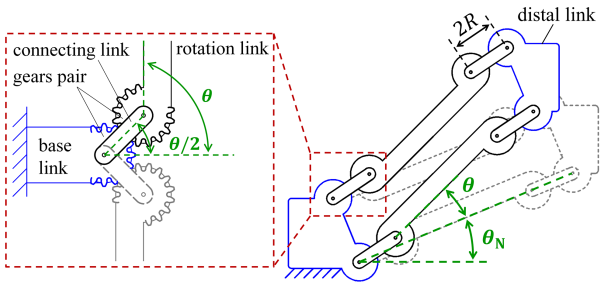

Fig. 1. Schematic diagram of a geared parallelogram with the different neutral angles when: $\theta_N = 22.5°$ and $\theta = 22.5°$.

simplifies the addition of electrical wiring and material supply to the distal links [17].

The rest of this article is organized as follows. Section II introduces the parallelogram mechanism based on geared rolling joints and analyzes the kinematics of the proposed palletizing robot with geared rolling joints. In Section III, an analysis of the cable-actuation for the parallelogram structure is described. This includes the effects of multiple cable windings and decoupled joint motion, along with a stiffness analysis. Section IV details the manufacturing of a prototype for the proposed palletizing robot, as well as the corresponding experiments and results. In addition, a discussion and a comparison between the results of theoretical simulations and experimental results are presented. Finally, Section V concludes this article.

II. Rolling-Based Parallelogram Mechanism

Parallelogram linkage is generally utilized in palletizing robots to handle large payloads. It enables the construction of a low-DOF robot arm, which maintains the orientation of the distal link during positioning movements. Fig. 1 shows the parallelogram linkage with rolling joints. Unlike the existing pivot joints with $R = 0$, the rolling joints consist of a pair of circles with a central distance of $2R$. These multi-axis rolling joints are joints that enable 1-DOF rotational movement between two axes [18]. Additionally, circular spur gears can be applied to prevent slippage on the rolling surfaces, which simplifies the design of the rolling joints [17], [19]. The angle of the connecting link, which maintains a constant distance between the two gears, is half the angle of the rotation link. Therefore, the distal link maintains a parallel structure with the base link. Meanwhile, in the design of a palletizing robot with geared parallelograms, it is important to consider the neutral posture. As depicted in the bottom right of the figure, the neutral posture is defined by the differences in the neutral angle of the parallelogram. Here, θ_{N} is a constant design parameter representing the angle between the rotation link and the horizontal plane when the rotation link angle θ is zero.

The kinematics of the proposed parallelogram, which includes the geared rolling joints, is complicated by the gear pitch circle radius [20]. When these joints are applied to a 4-DOF palletizing robot, its kinematics can be expressed using ten sets of Denavit–Hartenberg (DH) parameters based on the modified method, as given in Table I. Here, j_i represents the order of the local

TABLE I
DH Parameters for Rolling-Based Palletizing Robot

j_i	a_{i-1}	α_{i-1}	d_i	θ_i
1_1	-	-	d_1	θ_1
2_2	a_1	90	-	$\theta_2/2 + \theta_{\mathrm{N}_2}$
3_2	$2R_{\mathrm{J}}$	-	-	$\theta_2/2$
4_2	L_1	-	-	$-\theta_2/2$
5_2	$2R_{\mathrm{J}}$	-	-	$-\theta_2/2 - \theta_{\mathrm{N}_2}$
6_3	-	-	-	$-\theta_3/2 + \theta_{\mathrm{N}_3}$
7_3	$2R_{\mathrm{J}}$	-	-	$-\theta_3/2$
8_3	L_2	-	-	$\theta_3/2$
9_3	$2R_{\mathrm{J}}$	-	-	$\theta_3/2 - \theta_{\mathrm{N}_3}$
10_4	a_2	-90	-	θ_4

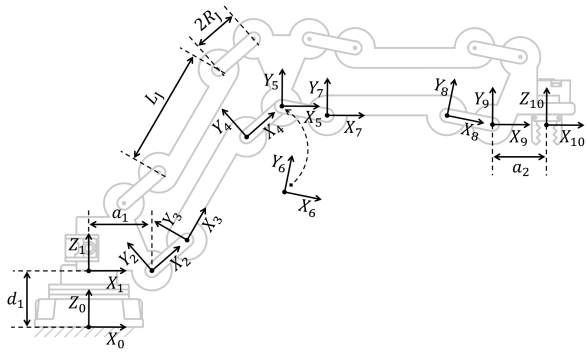

Fig. 2. Coordinate systems of the proposed palletizing robot for kinematic analysis.

coordinate systems, where j is the number of local coordinates, and i is the variable angle θ_i of the rotational link. L_J is the constant length of the long rotation link, and R_J is the radius of the gear pitch circle, which remains constant for each rolling unit joint in this robot. Additionally, θ_{N_i} represents the neutral angle, which is required only for the two parallelograms where the geared rolling joints are applied.

Fig. 2 shows the local coordinate systems for the kinematic analysis of this robot, which can be expressed using a homogeneous transformation matrix as follows:

$$ {}^{0}_{10}T = \begin{bmatrix} c_{14} & -s_{14} & 0 & p_x \\ s_{14} & c_{14} & 0 & p_y \\ 0 & 0 & 1 & p_z \\ 0 & 0 & 0 & 1 \end{bmatrix}. \tag{1} $$

The position elements can be calculated as follows:

$$ p_x = c_1 \left(a_1 + a_2 + L_1 c_{N2} + L_2 c_{N3} + 4R_J c_{N2/2} + 4R_J c_{N3/2}\right) \tag{2} $$

$$ p_y = s_1 \left(a_1 + a_2 + L_1 c_{\mathrm{N}2} + L_2 c_{N3} + 4R_J c_{N2/2} + 4R_J c_{N3/2}\right) \tag{3} $$

$$ p_z = d_1 + L_1 s_{N2} + L_2 s_{N3} + 4R_J s_{N2/2} + 4R_J s_{N3/2}. \tag{4} $$

Here, new parameters are adopted to simplify the expression as follows: $\theta_{ij} = \theta_{i+j}$; $s_i = \sin\theta_i$; $c_i = \cos\theta_i$; $s_{i/2} = \sin\theta_i/2$; $c_{i/2} = \cos\theta_i/2$; $c_{Ni} = c_{i+\theta_{N_i}}$; $s_{Ni} = s_{i+\theta_{N_i}}$;

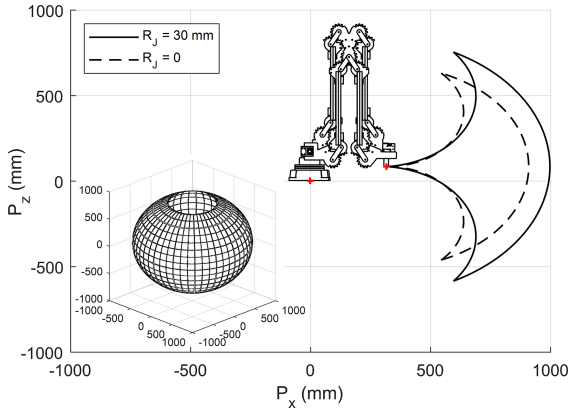

Fig. 3. Workspace analysis of the geared palletizing robot.

$c_{Ni/2} = c_{i/2+\theta_{N_i}}$; and $s_{Ni/2} = s_{i/2+\theta_{N_i}}$. Therefore, the distal position of the rolling-based palletizing robot is influenced by θ_{N_i} and R_J. Moreover, θ_4 is the angle of the distal wrist joint, which is kinematically independent of the robot's positional changes.

To analyze the positional accuracy of the proposed palletizing robot, it is necessary to perform inverse kinematics (IK) calculations. Although closed-form solutions are generally preferred for robots with simple structures, obtaining these solutions for a palletizing robot with rolling joints is very difficult. In such cases, a numerical approach using a Jacobian matrix can be applied. First, by taking the derivatives of (2)–(4) with respect to time, the following relation is satisfied:

$$[\dot{p}_x \;\; \dot{p}_y \;\; \dot{p}_z]^{\mathrm{T}} = \mathbf{J}(\Theta) \left[\dot{\theta}_1 \;\; \dot{\theta}_2 \;\; \dot{\theta}_3\right]^{\mathrm{T}}. \tag{5}$$

Here, the Jacobian matrix $\mathbf{J}(\Theta)$ indicates that the angular velocity of each rotational joint can be determined from the velocity of the distal link. In this relation, IK solutions are computed by iteratively reducing errors from nonlinearity for positional analysis. Therefore, the expression $[\dot{\theta}_1 \;\; \dot{\theta}_2 \;\; \dot{\theta}_3]^{\mathrm{T}} = \mathbf{J}^{-1}[\dot{p}_x \;\; \dot{p}_y \;\; \dot{p}_z]^{\mathrm{T}}$ can be used to numerically calculate the required rotation angle of each joint.

Fig. 3 shows the workspace of the proposed palletizing robot with planar coordinates and an isometric projection, as derived from (1). Here, the range of the rotation link angle is limited to $\pm 67.5°$, with neutral angles $\theta_{N_2} = +22.5°$ and $\theta_{N_3} = -22.5°$. The solid line represents the robot workspace with $R_J = 30$ mm, while the dashed line represents the workspace of the existing pivot joints with $R_J = 0$. Therefore, the analyzed position clarifies that the rolling joints, which include the additional design parameter R_J, represent a more comprehensive design.

III. Cable-Actuation Mechanism

A. Cable-Actuation of a Rolling-Based Parallelogram

As mentioned in Section II, the central axis of the rolling joint is not defined as a single axis. Therefore, a special mechanism is required for the geared parallelogram, where cables are applied selectively to some of the rolling joints. Fig. 4 depicts two

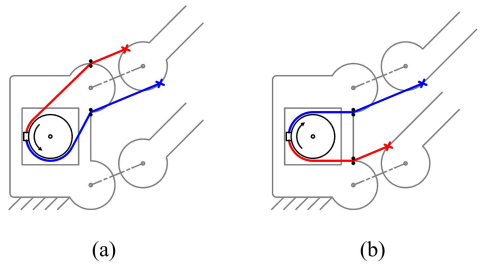

Fig. 4. Comparison of cable anchoring methods for a geared parallelogram. (a) Humped design with external cable routing. (b) Humpless design with internal cable routing.

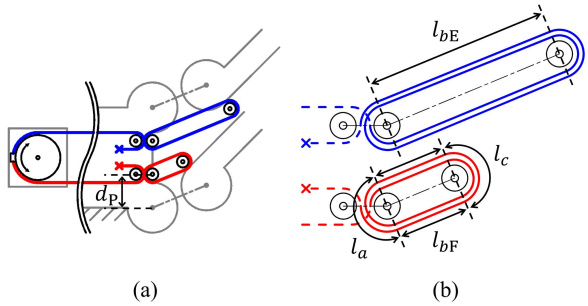

Fig. 5. Analysis of rotation link angle and cable length in humpless design. (a) Schematic of the cable windings. (b) Details of the cable lengths wound around multiple pulleys.

methods of cable anchoring for a parallelogram with rolling joints. The blue and red lines represent the cables for extension and flexion actuation, respectively. Fig. 4(a) and (b) depicts the "humped design" and "humpless design," respectively, where the cables are routed through the external and internal spaces of the parallelogram. Although the required motor rotation directions are different, these two cable anchoring methods provide the same actuation effect. Therefore, to save the robot volume, the humpless design can be adopted to construct the proposed palletizing robot. Meanwhile, the limited elasticity of a single actuation cable can be supplemented by wound around the multiple idle pulleys n_C times to reduce the joint speed [14], as shown in Fig. 5 ($n_C = 2$). When applying the joint angle θ_i with small idle pulleys located at a distance d_P from the center of the rolling joints, the total lengths of the cables between the two idle pulleys are

$$l_{bE} = 4n_C(R_J + d_P s_{i/2}) \tag{6}$$

$$l_{bF} = 4n_C(R_J - d_P s_{i/2}). \tag{7}$$

The amounts of cable actuation required for the joint angle θ_i can be expressed as follows: $\Delta l_{bE} = +4n_C d_P s_{i/2}$ and $\Delta l_{bF} = -4n_C d_P s_{i/2}$. On the other hand, the partial cable lengths l_a and l_c remain constant regardless of the joint angle θ_i to satisfy $n_C\,(l_a + l_c) = \text{constant}$. This relation is valid irrespective of the pulley radius because the sum of the winding angles of the cable around the pulleys remains constant even when the joint angle changes. Therefore, when the joints are in the neutral posture, the two actuation cable lengths are identical, and the resultant overall lengths of the winding cables l_E and l_F

are

$$l_E = l_{bE} + n_C\,(l_a + l_c) \tag{8}$$

$$l_F = l_{bE} + n_C\,(l_a + l_c)\,. \tag{9}$$

These relations confirm that the two actuation cables are completely symmetrical, and satisfy $\Delta l_E + \Delta l_F = 0$. Therefore, a single actuator can be used to actuate the joint with a circular spool of radius R_M to supply the cable actuation length of $\Delta l_M = \theta_M\ R_M$. Therefore, the motor rotation angle θ_M required for the joint rotation θ_i can be expressed as follows:

$$\theta_M = \frac{4 n_C d_P}{R_M}\, s_{i/2}. \tag{10}$$

Additionally, in a parallelogram, the angle of a unit joint is equal to that of another joint on the diagonally opposite side. The resultant speed reduction is determined by the sum of the cable windings n_C on the pair of unit joints. This arrangement of multiple cable windings results in a high reduction ratio and increased stiffness with a slim design.

B. Decoupled Joint Motion

When applying a cable actuation to the proposed palletizing robot, the driving motion of the actuator, located at the base part, must be transmitted accurately to the distal joints. However, if the actuation cable is routed improperly, it can limit the range of joint motion, leading to positional errors of the robot [21], [22]. Fig. 6 shows a cable routing passing through a via-joint schematically. In this parallelogram, the actuation cable passes diagonally across the two idle pulleys, which are concentric with the rolling gears. Therefore, as depicted in Fig. 6(b), the total cable length of the via-joint can be expressed as

$$L_V = \sum R_P \theta_{P_k} + \sum l_{d_k} + 2\sqrt{{R_J}^2 - {R_P}^2}. \tag{11}$$

Here, R_P represents the radius of the idle pulleys. θ_{P_k} is the partial winding angle of the cable on the pulleys, and l_{d_k} is the non-contact length of the cable segment between the pulleys, where k is the order of the partial cables. For counterclockwise rotation of the rotation link, as shown in Fig. 6(c), the partial length of the winding cable on the left pulley increases by $\theta_i/2$, while it decreases by $-\theta_i/2$ on the right one. Therefore, the total length of the actuation cable through the via-joint remains constant. Consequently, the driving motion of the actuator can be transmitted to the distal goal joint regardless of the motion of the intermediate via-joints.

Palletizing robots can be assembled effectively by using two of the proposed parallelograms. In the elbow-up position, the upward movement is controlled by θ_2 at the first proximal joint, while the second distal joint moves downward by $-\theta_3$. Fortunately, using geared unit joints ensures that the distal joint is not affected by the motion of the intermediate via-joints. Accordingly, the serially connected geared parallelograms do not affect each other, and their motions can be decoupled completely. Fig. 7 shows the routes of the actuation cables in the two serially connected geared parallelograms schematically. Here, the base

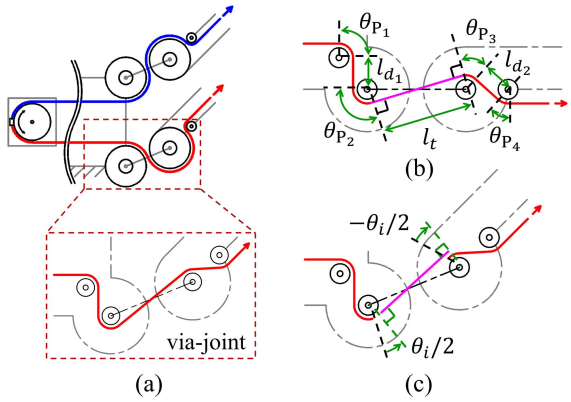

Fig. 6. Schematics of the cable routing passing through a via-joint. (a) Pulley disposition for a constant cable length, (b) the partial cable length in the neutral posture. (c) Total cable length in the rotational posture.

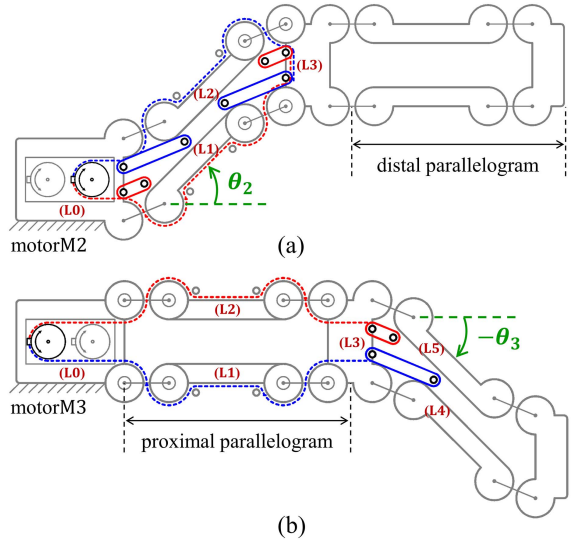

Fig. 7. Conceptual design of a cable-actuated parallelogram linkages with the rotation link angles. (a) θ_2 and (b) θ_3.

and middle links are represented by $L0$ and $L3$, respectively; $L1$ and $L4$ denote the lower rotation links, and $L2$ and $L5$ represent the upper rotation links. The solid lines represent the partial cables, whose variable lengths between the links Li and Lj are l_{Eij} and l_{Fij}, as calculated in (8) and (9). On the other hand, the dashed lines represent other partial cables with constant lengths, including L_{Li} on link Li and L_{Vij} at the via-joint between Li and Lj.

The actuation cable for rotating the first parallelogram starts from motor $M2$ on link $L0$, passes through links $L1$ or $L2$, after winding around the idle pulleys, and then winding around once again before being fixed to link $L3$. Similarly, the actuation cable for the second parallelogram passes through the first parallelogram including the middle link $L3$, and then winding around the idle pulleys on links $L4$ or $L5$ before being fixed to link $L3$. Therefore, the total length of the extension and flexion cables of the proximal and distal parallelograms can be expressed as

follows:

$$L_{\mathrm{CE}}(\theta_2) = L_{L0} + l_{E02} + L_{\mathrm{V02}} + L_{L2} + L_{\mathrm{V23}} + L_{L3} + l_{E31} \tag{12}$$

$$L_{\mathrm{CF}}(\theta_2) = L_{L0} + l_{F01} + L_{V01} + L_{L1} + L_{\mathrm{V13}} + L_{L3} + l_{F32}, \tag{13}$$

$$L_{\mathrm{CE}}(\theta_3) = L_{L0} + L_{V01} + L_{L1} + L_{V13} + L_{L3} + l_{E34}, \tag{14}$$

$$L_{\mathrm{CF}}(\theta_3) = L_{L0} + L_{V02} + L_{L2} + L_{V23} + L_{L3} + l_{F35}. \tag{15}$$

Thus, based on the neutral posture with $\theta_i = 0°$, the cable actuation lengths are determined as follows: $\Delta L_{\mathrm{CE}}\ (\theta_i) = +4n_{\mathrm{C}}d_{\mathrm{P}}s_{i/2}$ and $\Delta L_{\mathrm{CF}}\ (\theta_i) = -4n_{\mathrm{C}}d_{\mathrm{P}}s_{i/2}$. Consequently, the cable actuation required for the second parallelogram is unaffected by the change in θ_2. This means that each actuation of the two parallelograms can be decoupled completely.

C. Stiffness Analysis

The stiffness of the geared parallelogram is analyzed schematically, as shown in Fig. 8. All components are assumed to be rigid bodies, except for the actuation cables. The friction between the cables and pulleys is also ignored. When the motor rotates clockwise, the relationship between the cable tension T_M due to the motor and the virtually amplified tension T_P resulting from the cables winding around the idle pulleys can be expressed as follows: $T_P = 2n_C T_M$. Additionally, the relationship between the linear displacement near the motor Δx_M and the change in distance between the idle pulleys Δx_P, which amplifies the tension, can be expressed as: $\Delta\, x_P = \Delta x_M / 2n_C$. Therefore, through the multiple cable windings, the cable tension is amplified, leading to a reduction of the joint speed to $1/2n_C$. Moreover, when the cables are composed of multi-stranded elastic materials, the cable stiffness K_C can be approximated as

$$K_C \approx \frac{C_C C_E C_A}{L_{\mathrm{total}}}. \tag{16}$$

Here, C_E and C_A represent the elastic modulus and cross-sectional area of the cable, respectively. On the other hand, C_C is introduced as a correction factor to calculate the cable stiffness, and it is set to zero for the initial prediction without experimental results. The total length of each pulling cable L_{total} is calculated as follows:

$$L_{\mathrm{total}} = L_{MJi} + 4n_C(R_J + d_P s_{i/2}) + n_C\,(l_a + l_c)\,. \tag{17}$$

This relation indicates that K_C is inversely proportional to the total length of each pulling cable L_{total}. Here, L_{MJi} represents the constant length of the cable from the motor to the joint, and i is the variable angle θ_i of the rotation links of the first and second parallelograms. Fig. 9 shows the relationship between $L_{\mathrm{MJ}i}$ and K_{C}. Here, L_{MJi} ranges from 100 to 1000 mm, and $n_C = 1, 2, 4$, and 6. The following values are used for the calculation: $d_P = 40$ mm; $R_J = 30$ mm; $\theta_i = 0°$; $C_E = 200$ GPa; and $C_A = 0.789$ mm^2. The results indicate that K_C is nearly inversely proportional to L_{MJi}. Thus, when L_{MJi} is large, n_C does not significantly affect the cable stiffness K_C.

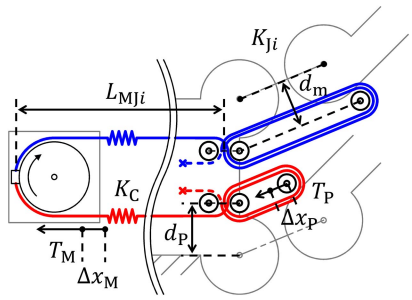

Fig. 8. Schematic diagram for the stiffness analysis of a parallelogram.

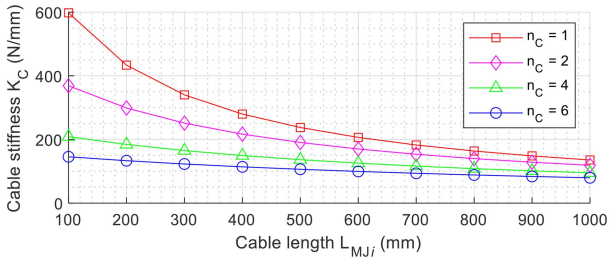

Fig. 9. Relationship between the cable stiffness K_C and cable length L_{MJi}.

Meanwhile, d_m, which represents the average distance between the actuation cables and center of the rotation axes, can be expressed as $d_m = d_P\ c_{i/2}$. If a small rotational displacement $\Delta\theta_i$ is applied without motor rotation, the amplified cable tensions for flexion and extension can be calculated as follows:

$$T_F = K_C\ (L_{\mathrm{pre}} + 2n_C d_m \Delta\theta_i) \tag{18}$$

$$T_E = K_C\ (L_{\mathrm{pre}} - 2n_C d_m \Delta\theta_i)\,. \tag{19}$$

Here, L_{pre} represents the pretensioned cable length. Then, the external torque $\Delta\tau_{\mathrm{J}}$ generated by these cable tensions is applied to the joint as

$$\Delta\,\tau_J = n_C\ d_m\,(T_F - T_E)\,. \tag{20}$$

Therefore, the resultant joint stiffness $K_{Ji} = \Delta\tau_J / \Delta\theta_i$, can be expressed using (18) and (19) as follows: $K_{Ji} = 4K_C\ {n_C}^2 {d_i}^2$. By substituting (16) and (17), the following expression can be obtained:

$$K_{Ji} = \frac{4C_E C_A {n_C}^2 {d_P}^2 {c_{i/2}}^2}{L_{MJi} + 4n_C(R_J + d_P s_{i/2}) + n_C\,(l_a + l_c)}\,. \tag{21}$$

Additionally, when an external force F_Z is applied in the Z-direction on the distal link of the serially connected 2-DOF parallelograms, the linear distal displacement ΔZ of the robot arm will be

$$\Delta Z = \frac{F_Z L_2^2 c_2^2}{K_{J2}} + \frac{F_Z L_3^2 c_3^2}{K_{J3}}. \tag{22}$$

The Z-directional linear robot stiffness K_{RZ} can be defined as: $K_{RZ} = F_Z\ / \Delta Z$. In this relation, the Z-directional total linear compliance C_{RZ} of the proposed robot is achieved by adding the compliance of two parallelograms. It can be calculated as the reciprocal of the robot stiffness, as follows:

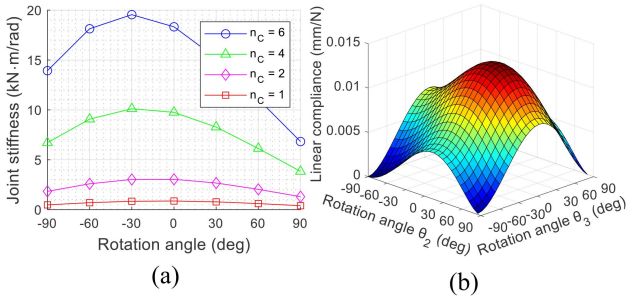

Fig. 10. (a) Analysis of the relationship between the rotation link angle and joint stiffness of a 1-DOF parallelogram with $L_{MJi} = 1000$ mm and (b) Analysis of the *Z*-directional linear compliance for various postures of the proposed palletizing robot with $L_{MJ2} = 100$ mm and $L_{MJ3} = 1000$ mm.

$C_{RZ} = (L_2^2 c_2^2/K_{J2}) + (L_3^2 c_3^2/K_{J3})$. By substituting (21), the following calculation can be derived:

$$C_{RZ} = \frac{L_2^2 c_2^2}{\frac{4C_C C_E C_A n_C{}^2 d_P{}^2 c_{i/2}{}^2}{L_{MJ2}+4n_C(R_J+d_P s_{i/2})+n_C(l_a+l_c)}} + \frac{L_3^2 c_3^2}{\frac{4C_C C_E C_A n_C{}^2 d_P{}^2 c_{i/2}{}^2}{L_{MJ3}+4n_C(R_J+d_P s_{i/2})+n_C(l_a+l_c)}}. \quad (23)$$

Consequently, this robot can estimate ΔZ at a specific posture when an external force is applied, using (21)–(23). This calculation enables the prediction of cable deformation based on the number of cable windings n_C. Fig. 10(a) shows the relationship between the rotation link angle and the joint stiffness of a parallelogram. Here, L_{MJi} is 1000 mm, $\theta_i = [-90°, 90°]$, and the other parameters are the same as those in Fig. 9. If L_{MJi} is very long, the joint stiffness is approximately proportional to the square of n_C for the complete range of θ_i; the maximum stiffness is achieved in the neutral posture of the joint where $\theta_i = 0°$.

Fig. 10(b) shows the Z-directional linear compliance for various postures of the proposed palletizing robot, where $n_C = 4$ was applied for the first and second parallelograms, respectively. The following values are used for the calculation: $L_J = 300$ mm, $L_{MJ2} = 100$ mm, $L_{MJ3} = 1000$ mm, and other parameters are the same as those shown in Fig. 10(a). These two simulation results confirm that the values of the cable windings n_C and the cable length L_{MJi} applied to the geared parallelograms can affect the overall stiffness of the proposed palletizing robot. Therefore, the importance of selecting the appropriate values for n_C and L_{MJi} in the initial design of the proposed palletizing robot.

IV. Experimental Validation and Discussion

A prototype was designed to experimentally verify the cable-actuated palletizing robot, as shown in Fig. 11. Most commercialized mechanical components were procured from MISUMI Korea, and a Markforged 3-D printer using Onyx material with micro carbon fiber was utilized to manufacture all nonstandardized components. This robot prototype's total weight was 4.1 kg, and the weight of the actuation links were 1.3 and 1.1 kg

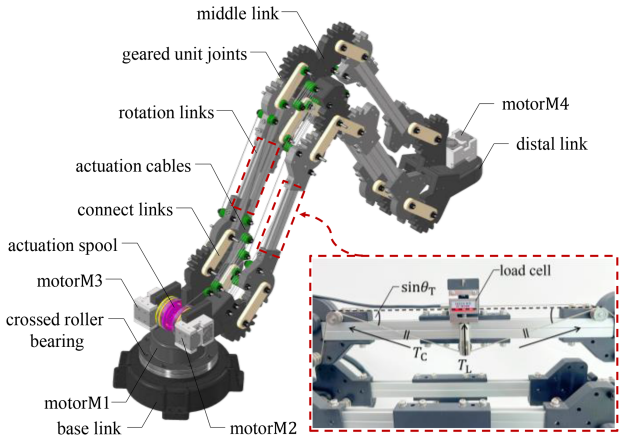

Fig. 11. Prototype design of the proposed palletizing robot with a cable tension measurement sensor.

for the first and second parallelograms, respectively. Moreover, a Dynamixel XH430-W350-R motor with a 3.4 N · m stall torque was used. To improve the robot stability, a crossed roller bearing was applied at the base part. The utilized transmission cable was made of SS304 with an ultimate tensile strength of 1570 N/mm^2, a diameter of 1.0 mm, and a 7 × 19 construction. The following design parameters were applied to this robot: $\theta_{N_2} = +22.5°, \theta_{N_3} = -22.5°, L_J = 300$ mm, $R_J = 30$ mm, $R_M = 25$ mm, $d_P = 40$ mm, $L_{MJ2} = 250$ mm, $L_{MJ3} = 750$ mm, respectively. Meanwhile, in this current robot design, the actuation ranges of the rotation links are limited to ±67.5° to prevent collisions of components.

A. Effect of Multiple Cable Windings

To verify the effect of the multiple cable windings, the motor $M2$ torque of the first parallelogram was measured when driving θ_2 without changing θ_3. Subsequently, the motor $M3$ torque of the second parallelogram was measured when driving θ_3 without changing θ_2. The parallelograms were actuated five times at a low rotational speed of 13.7 deg/sec in the range of ±67.5°. In Fig. 12, the red, blue, and green lines represent the motor torques measured for three different numbers of cable windings n_{Ci}. The dotted lines represent the theoretical motor torque predicted by applying the weight of this robot prototype. The value for the first proximal parallelogram, n_{C1} was determined by the sum of the cable windings on the pair of diagonally opposite sides. For the upward motion, the root mean square torques of the first parallelogram were measured as [0.749, 0.588, 0.441 N · m], and for the second parallelogram were measured as [0.751, 0.538, 0.442 N · m], respectively. When comparing the predicted motor torque values based on the robot's weight with the experimentally measured values, the resultant root mean square errors (RMSE) of the motor torques were [0.1901, 0.1863, 0.1843 N · m] and [0.1721, 0.1827, 0.1811 N · m], respectively.

The measured motor torque results indicated that the root mean square torques during upward motion decreased by an average of 41.12% and 41.15% for the first and second parallelograms, respectively, in a comparison between the largest and smallest numbers of cable windings. Additionally, to compare

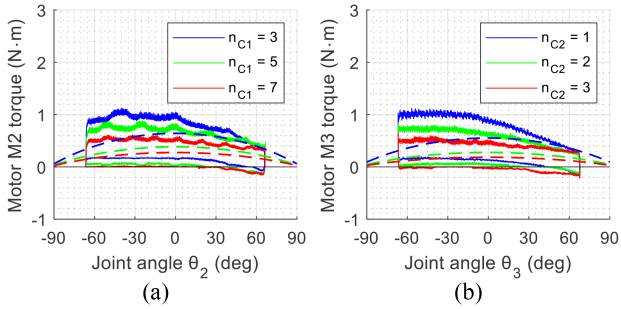

Fig. 12. Relationship between the cable windings and the required motor torques for the (a) first parallelogram and (b) second parallelogram.

the measured motor torques with the theoretical values, the RMSEs averaged 0.1869 and 0.1789 $\mathrm{N \cdot m}$, indicating no significant difference. Therefore, despite using a low-torque motor, the cable tension was amplified successfully with a speed reduction effect was achieved by the multiple cable windings at the joints, as explained in Section III-A. However, the motor torque was not entirely proportional to the number of cable windings n_C. This issue might have been caused by the sliding friction between the gear teeth and the rolling friction between the cable and idle pulleys in the multiple joints.

B. Decoupled Joint Motion

In Fig. 11, the red box illustrates the measurement of the cable tension T_C, which is converted from the measured force T_L on the load cell as: $T_L = 2T_C \sin\theta_T$. Each parallelogram was actuated independently five times at a low rotational speed of 13.7 $\mathrm{deg/sec}$ within a range of $\pm 67.5°$, while the other was paused. As shown in Fig. 13, a cable pre-tension of 7.3 N was applied, with the cable windings of $n_{C1} = 5$ and $n_{C2} = 2$. The black dashed line represents the rotation link angles θ_i, while the red and blue lines indicate the measured cable tension T_{Ci}. Here, the theoretical values of the cable tension were equal to the cable pre-tension. As a result, the minimum and maximum values of cable tension changes for the two parallelograms were measured as $[-0.7361, 0.7285\ \mathrm{N}]$ and $[-0.7771, 0.3628\ \mathrm{N}]$, respectively.

In these results, the tension changes in the two actuation cables were not symmetrical. This asymmetry could be attributed to the friction caused by the numerous idle pulleys used for cable routing. The first proximal parallelogram involved more pulleys than the second one, particularly when a large n_C was required. This led to an accumulation of friction and reduced symmetrical changes in cable tension. However, even though the motor torque increased during the upward motion, the tension changes resulting from the other parallelogram did not exceed ± 0.8 N. This means that the joint motion can be nearly decoupled, as explained in Section III-B.

C. Robot Stiffness

To evaluate the effect of multiple cable windings on the robot stiffness, the *Z*-directional distal displacements for various weights were measured while the robot was in a static posture.

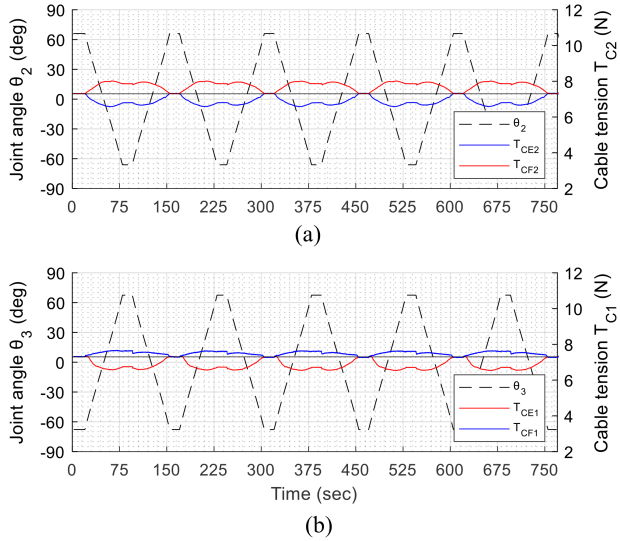

Fig. 13. Measured cable tensions for the repeated joint actuation test: The influence of (a) θ_2 on T_{C2} and (b) θ_3 on T_{C1}.

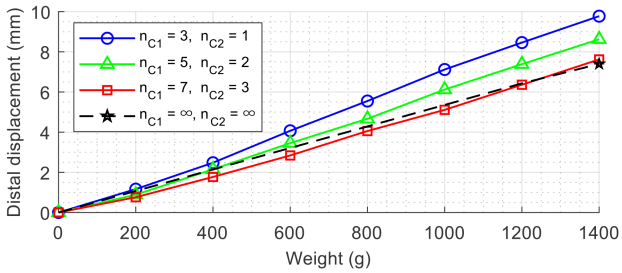

Fig. 14. Measurement of distal displacements for various weights with the different number of cable windings.

In Fig. 14, three different lines represent the measured distal displacements for the weights located on the distal link, with rotational link angles of $\theta_2 = 22.5°$ and $\theta_3 = -22.5°$ achieved by fixing the motor angles. For comparison, the black dotted line shows the predicted distal displacement when the value of n_C is infinite. The true distal position of the distal link was measured using the IRIS motion tracker from PS-TECH with IR-markers. Consequently, when a weight of 1400 g was applied, the resultant distal displacements for the three cases were measured as 9.77, 8.62, and 7.61 mm, as given in Table II.

By comparing the measured distal displacement with the theoretical value calculated in (22), it is confirmed that the experimental values were larger. This discrepancy can be attributed to the deformation of the link components and cables in this robot prototype. The pseudoinverse matrix was utilized to calculate the deformation of the link and cables when a weight of 1400 g was applied. This allowed for the estimation of the displacement when n_C was infinite. Consequently, the cable stiffness predicted from the simulation was calculated to be approximately three times greater than the corrected cable stiffness deduced from the robot prototype, as given in Table II. Additionally, the distal displacement due to the link's deformation is predicted to be approximately 7 mm in three cases. The deformation of this link is considered to result from the low stiffness of the

TABLE II
Z-DIRECTIONAL DISTAL DISPLACEMENT OF PALLETIZING ROBOT

Distal Displacement ΔZ (mm)			
$n_{C1} : n_{C2}$	Simulation	Experiment	
		Measured	Corrected
3 : 1	0.69	9.77	2.29
5 : 2	0.22	8.62	0.71
7 : 3	0.12	7.61	0.37
∞ : ∞	-	-	0.00

3-D-printed components of the robot prototype, even though they were reinforced with microcarbon fibers. To improve this, the manufactured components could be replaced with metallic materials. Meanwhile, in the current design, the lengths of L_{MJi} for the first and second parallelograms were relatively short, at 250 and 700 mm, respectively. Therefore, the joint stiffness was not proportional to the square of n_C, as described in (21)–(23).

D. Accuracy of Distal Position and Orientation

Fig. 15 shows additional experiments that confirm the robot's performance in terms of position accuracy and orientation accuracy in both the lateral and frontal planes. The blue dashed line represents the theoretical value of a 200 mm square, which is expected to be the most frequently used area within the robot's workspace. Additionally, Fig. 15(a) shows the actual size of the robot, which is longer than the length of a human arm. An inertial measurement unit sensor and a motion tracker were utilized to measure the orientation and obtain positional information of the distal link, respectively. To quantitatively analyze the distal position, the robot was actuated to move along points P_j, as shown in Fig. 16. The palletizing robot was actuated clockwise five times at a rotational speed of 13.7 deg/sec, with the cable windings of $n_{C1} = 5$ and $n_{C2} = 2$.

In Fig. 16(a) and (b), the red lines indicate the measured distal position. The resultant positional RMSEs for points P_j measured in the two planes were averaged [2.4986, 1.4396, 5.6513, 3.3142 mm] and [4.4871, 4.6083, 5.8419, 4.9693 mm]. These positional errors can occur in extended robot postures due to cable elongation. The errors could be mitigated by increasing the number of cable windings to prevent excessive tension changes. Additionally, the repeatability of the measured positions is given in Table III. Resultantly, the positional standard deviations for measured points P_j in the two different planes were averaged at 0.0075 and 0.0185 mm, respectively. These results can satisfy the repeatability requirements for most industrial robots, even when using cables and without the need for expensive speed reducers.

Meanwhile, to verify that the distal link maintains a horizontal orientation, the 'roll' and 'pitch' angles, which are directly affected by the robot operation, were measured. In Fig. 16(c) and (d), the red and green lines represent the measured roll and pitch angles of the distal link. The resultant angular RMSEs for the entire path in the two planes were averaged at [0.6742°, 0.0351°] and [0.4732°, 0.0607°], respectively. These results show that the operational performance of the palletizing robot was little influenced, and the horizontal orientation of the distal link could be effectively maintained.

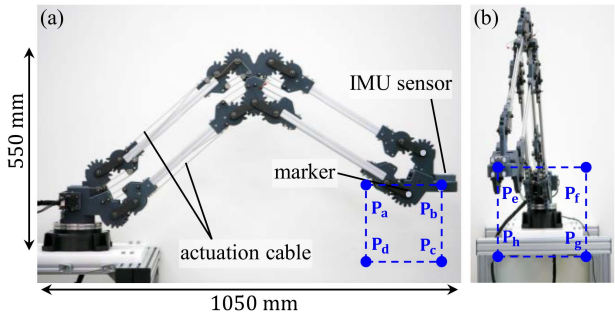

Fig. 15. Various postures to verify the actuation test. (a) Lateral plane and (b) frontal plane.

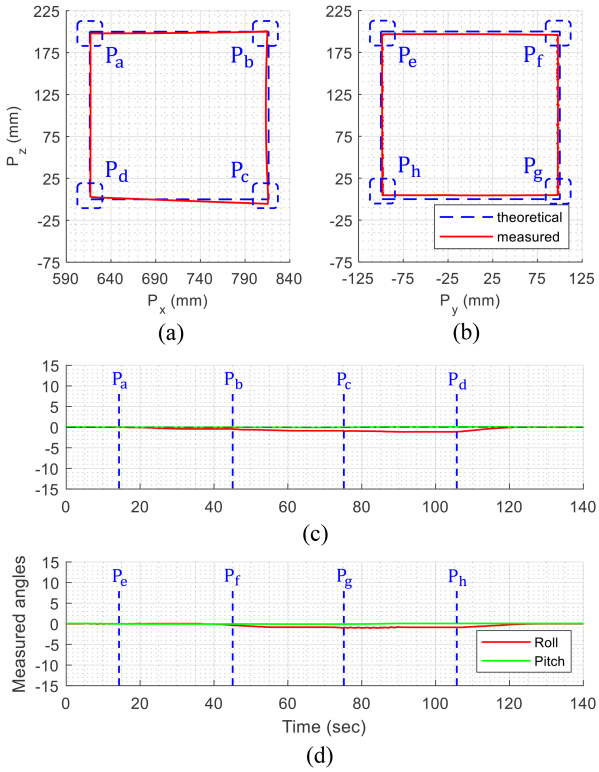

Fig. 16. Measurement results of positional accuracy. (a) and (b) Measured distal position. (c) and (d) Measured distal orientation.

TABLE III
DISTAL POSITIONAL REPEATABILITY OF PALLETIZING ROBOT

Measured Repeatability				
Standard Deviation (mm)	$\mathrm{P_a}$	$\mathrm{P_b}$	$\mathrm{P_c}$	$\mathrm{P_d}$
	0.0061	0.0056	0.0169	0.0016
	$\mathrm{P_e}$	$\mathrm{P_f}$	$\mathrm{P_g}$	$\mathrm{P_h}$
	0.0014	0.0122	0.0058	0.0547

V. CONCLUSION

In this article, to improve the structure of the palletizing robot, the cable-actuated parallelograms with geared rolling joints were applied. These serially connected parallelograms offer a

compromised design that balances between the robot stiffness and a lightweight structure, with cable-actuation serving as an intermediate solution. To achieve a desirable robot design, the kinematics related to the robot's distal position and workspace were analyzed. Moreover, the relationship between the joint angle and cable length, the effect of the multiple cable windings, and the decoupling of joint motion were theoretically analyzed.

The proposed palletizing robot was experimentally validated using a manufactured prototype composed of 3-D-printed components reinforced with microcarbon fiber material. In the experimental results, cable tension was successfully amplified through multiple cable windings. Additionally, the serially connected geared parallelograms could be actuated individually. This decoupling of joint motion significantly simplifies electrical wiring or material supply to the distal links. Therefore, with an appropriate number of cable windings and other design parameters, it is possible to achieve performance comparable to that of the existing industrial robots. Meanwhile, the proposed palletizing robot offers significant design advantages by simplifying the structure of parallel robots. This approach strategically places actuators in the base part, providing a foundation for incorporating additional wrist joints or end effectors into various parallel robots. In conclusion, the proposed palletizing robot with geared parallelograms contributes to a lightweight and slim robot design, which has the potential to replace the small robotic arms currently utilized for pick-and-place operations in logistics and production lines. Therefore, the proposed cable-actuated palletizing robot is expected to significantly contribute to the development of industrial robots.

References

[1] B. R. Vemula, G. Spampinato, M. Hedelind, X. Feng, and T. Brogårdh, "Structural synthesis of 3DOF articulated manipulators based on kinematic evaluation," in *Proc. 16th Int. Conf. Adv. Robot.*, 2013, pp. 1–7.

[2] L. Liang, Y. Liu, H. Han, M. Wu, and Q. Ma, "A method of structure optimization for high-speed and heavy-load robot based on dynamic characteristic analysis," in *Proc. IEEE Int. Conf. Adv. Intell. Mechatronics*, 2016, pp. 1461–1466.

[3] Z. Liu, J. Wu, L. Wang, and B. Zhang, "Control parameters design based on dynamic characteristics of a hybrid robot with parallelogram structures," *IEEE/ASME Trans. Mechatronics*, vol. 26, no. 2, pp. 1140–1150, Apr. 2021.

[4] C. Scheurer and U. E. Zimmermann, "Path planning method for palletizing tasks using workspace cell decomposition," in *Proc. IEEE Int. Conf. Robot. Automat.*, 2011, pp. 1–4.

[5] H. Shao, Y. Wang, X. Li, X. Wang, and F. Song, "Structural design of a kind of palletizing robot with double-drive mechanical-arm and large lifting force," in *Proc. IEEE Int. Conf. Real-Time Comput. Robot.*, 2017, pp. 133–138.

[6] W. Lee, D. Kim, and J. Song, "Novel 3-DOF counterbalance mechanism based on spring balancer for mobile robot arms," *Mechatronics*, vol. 82, Apr. 2022, Art. no. 102734.

[7] A. Tai, M. Chun, Y. Gan, M. Selamet, and H. Lipson, "Para: A onemeter reach, two-kg payload, three-DOF open source robotic arm with customizable end effector," *HardwareX*, vol. 10, Oct. 2021, Art. no. e00209.

[8] Y.-J. Kim, S. Cheng, S. Kim, and K. Iagnemma, "A stiffness-adjustable hyper redundant manipulator using a variable neutral-line mechanism for minimally invasive surgery," *IEEE Trans. Robot.*, vol. 30, no. 2, pp. 382–395, Apr. 2014.

[9] J. Suh, "Utilization of 2N + 1 units for 2-dof discrete bending joint to transmit perfect axial rotation for laparoscopic instruments," *Int. J. Control, Automat. Syst.*, vol. 18, no. 1, pp. 186–195, Nov. 2020.

[10] H. Sun, Y. Zhang, B. Xie, and B. Zi, "Dynamic modeling and error analysis of a cable-linkage serial-parallel palletizing robot," *IEEE Access*, vol. 9, pp. 2188–2200, 2021.

[11] T. Lens and O. von Stryk, "Design and dynamics model of a lightweight series elastic tendon-driven robot arm," in *Proc. IEEE Int. Conf. Robot. Automat.*, 2013, pp. 4512–4518.

[12] W. Li, Y. Wang, S. Togo, H. Yokoi, and Y. Jiang, "Development of a humanoid shoulder based on 3-motor 3 degrees-of-freedom coupled tendon-driven joint module," *IEEE Robot. Automat. Lett.*, vol. 6, no. 2, pp. 1105–1111, Apr. 2021.

[13] D. Lee and T. Seo, "Lightweight multi-DOF manipulator with wire-driven gravity compensation mechanism," *IEEE/ASME Trans. Mechatronics*, vol. 22, no. 3, pp. 1308–1314, Jun. 2017.

[14] Y.-J. Kim, "Anthropomorphic low-inertia high-stiffness manipulator for high-speed safe interaction," *IEEE Trans. Robot.*, vol. 33, no. 6, pp. 1358–1374, Dec. 2017.

[15] S. Pang, W. Shang, F. Zhang, B. Zhang, and S. Cong, "Design and stiffness analysis of a novel 7-dof cable-driven manipulator," *IEEE Robot. Automat. Lett.*, vol. 7, no. 2, pp. 2811–2818, Apr. 2022.

[16] M. Wang, B. Liao, and Y. Lou, "Accuracy analysis and optimal design of palletizing robot with joint clearance," in *Proc. IEEE Int. Conf. Real-time Comput. Robot.*, 2017, pp. 355–360.

[17] J. Suh and W. Choi, "Design and verification of parallelogram mechanism with geared unit rolling joints for reliable wiring," *IEEE Robot. Automat. Lett.*, vol. 8, no. 6, pp. 3756–3763, Jun. 2023.

[18] J.-W. Suh, K.-Y. Kim, J.-W. Jeong, and J.-J. Lee, "Design considerations for a hyper-redundant pulleyless rolling joint with elastic fixtures," *IEEE/ASME Trans. Mechatronics*, vol. 20, no. 6, pp. 2841–2852, Dec. 2015.

[19] R. Ozawa, Y. Mishima, and Y. Hirano, "Design of a transmission with gear trains for underactuated mechanisms," *IEEE Trans. Robot.*, vol. 32, no. 6, pp. 1399–1407, Dec. 2016.

[20] C. L. Collins, "Kinematics of robot fingers with circular rolling contact joints," *J. Robot. Syst.*, vol. 20, no. 6, pp. 285–296, Jun. 2003.

[21] D. Shah, A. Parmiggiani, and Y.-J. Kim, "Constant length tendon routing mechanism through axial joint," in *Proc. IEEE/ASME Int. Conf. Adv. Intell. Mechatronics*, 2020, pp. 753–758.

[22] S. Jiang, D. Hua, Y. Wang, F. Ju, L. Yin, and B. Chen, "Design and modeling of motion-decoupling mechanism for cable-driven joints," *Adv. Mech. Eng.*, vol. 10, no. 5, pp. 1–10, May 2018.

Wontae Choi (Student Member, IEEE) received the B.S. degree in computer science and the M.S. degrees in robot and smart system engineering from the Kyungpook National University (KNU), Daegu, South Korea, in 2022 and 2024, respectively.

He is currently an Associate Researcher with the Department of Robot and Smart System Engineering, KNU, Daegu, South Korea. His research interests include robotics, co-manipulation, humanoid robots, physical human–robot interaction, and mechanism design for various devices and robots.

Jungwook Suh (Member, IEEE) received the B.S., M.S., and Ph.D. degrees in mechanical engineering from the Korea Advanced Institute of Science and Technology, Daejeon, South Korea, in 2007, 2009, and 2013, respectively.

From 2014 to 2019, he was a Senior Researcher with the Electronics and Telecommunications Research Institute, Daejeon, South Korea. He is currently an Associate Professor with the Department of Robot and Smart System Engineering, Kyungpook National University, Daegu, South Korea. His research interests include robotics and mechanism design for various devices and robots.